

# Revisit of the Occurrence of the Kuroshio Large Meander South of Japan

BO QIU<sup>a</sup> AND SHUIMING CHEN<sup>a</sup>

<sup>a</sup> *Department of Oceanography, University of Hawai'i at Mānoa, Honolulu, Hawaii*

(Manuscript received 2 August 2021, in final form 2 November 2021)

**ABSTRACT:** A unique characteristic by the Kuroshio off the southern coast of Japan is its bimodal path variations. In contrast to its straight path that follows the coastline, the Kuroshio takes a large meander (LM) path when its axis detours southward by as much as 300 km. Since 1950, eight Kuroshio LM events took place and their occurrences appeared random. By synthesizing available in situ/satellite observations and atmospheric reanalysis product, this study seeks to elucidate processes conducive for the LM occurrence. We find neither changes in the inflow Kuroshio transport from the East China Sea nor in the downstream Kuroshio Extension dynamic state are determinant factors. Instead, intense anticyclonic eddies with transport  $> 20$  Sv ( $1 \text{ Sv} \equiv 10^6 \text{ m}^3 \text{ s}^{-1}$ ) emanated from the Subtropical Countercurrent (STCC) are found to play critical roles in interacting with Kuroshio path perturbations southeast of Kyushu that generate positive relative vorticities along the coast and lead the nascent path perturbation to form a LM. Occurrence of this intense cyclonic–anticyclonic eddy interaction is favored when surface wind forcing over the STCC is anticyclonic during the positive phasing of Pacific decadal oscillations (PDOs). Such wind forcing strengthens the meridional Ekman flux convergence and enhances eddy generation by the STCC, and seven of the past eight LM events are found to be preceded by 1–2 years by the persistent anticyclonic wind forcings over the STCC. Rather than a fully random phenomenon, we posit that the LM occurrence is regulated by regional wind forcing with a positive PDO imprint.

**KEYWORDS:** Boundary currents; Mesoscale processes; Pacific decadal oscillation; Climate variability

## 1. Introduction

Originating from the bifurcated North Equatorial Current (NEC) off the Philippine coast near  $12^\circ\text{N}$  at surface, the Kuroshio is the western boundary current of the wind-driven subtropical gyre in the North Pacific Ocean (see Imawaki et al. 2013; Qiu 2019 for recent reviews). The Kuroshio gains its strength and transport as it flows poleward with the island of Luzon, the island of Taiwan, and the steep continental slope of the East China Sea serving as an effective western boundary (Fig. 1a). The mean Kuroshio transport east of Luzon across  $18^\circ\text{N}$ , for example, has been observed to be  $\sim 15$  Sv (Lien et al. 2014) and that across the East China Sea continental slope near  $28^\circ\text{N}$  to be  $\sim 24$  Sv (e.g., Ichikawa and Beardsley 1993; Andres et al. 2008). Due to the constraint of the side boundary, the upstream Kuroshio path from east of Luzon to the East China Sea is comparatively stable. One exception occurs around the Luzon Strait and east of Taiwan where the Kuroshio path and transport can deviate significantly from the means due to impinging mesoscale eddies generated from the unstable Subtropical Countercurrent (STCC) (e.g., Zhang et al. 2001; Gilson and Roemmich 2002; Hsin et al. 2013; Chang et al. 2015; Cheng et al. 2017; Jan et al. 2017; Andres et al. 2017; Chang et al. 2018).

The Kuroshio veers eastward and enters the deep Shikoku Basin through the Tokara Strait south of Kyushu (Fig. 1b). Due to the added mass influx from the Ryukyu Current, the mean net transport of the Kuroshio south of Japan increases to  $\sim 42$  Sv (Imawaki et al. 2001). This transport value agrees roughly with the maximum Sverdrup transport for the wind-driven subtropical gyre across the North Pacific (Risien and Chelton 2008). Near  $139^\circ\text{E}$ , the Kuroshio encounters the meridionally oriented

Izu Ridge. Its presence restricts the Kuroshio to exit the Shikoku Basin either through a deep passage near  $34^\circ\text{N}$  or south of  $33^\circ\text{N}$ , where the ridge height drops (Qiu and Chen 2005, their Fig. 11).

Due to the topographic constraints at its inflow and outflow locations, the Kuroshio path south of Japan is known for its bimodal path fluctuations (Kawabe 1995). As depicted in Fig. 1b, during the “straight path” years like 2010–12, the Kuroshio flows closely along the southern coast of Japan, while in the “large meander” years such as 2018–20, the Kuroshio takes a southward detoured path from  $135^\circ$  to  $140^\circ\text{E}$ . Kuroshio large meander (hereafter LM) has been observed to occur highly irregularly; for example, while four consecutive LM events took place from the mid-1970s to the early 1990s, only one LM event was detected from the mid-1990s to mid-2010s.

Theoretical and modeling studies attempting to explain the bimodal Kuroshio path variations have a long history. As with regard to other natural phenomena, our understanding on the Kuroshio LM occurrence depended on the number of events and the observational capabilities at the time the investigations were pursued. Most studies before 2000 have focused on the dependence of LM occurrence on the inflow Kuroshio condition in the East China Sea, and common themes explored then included roles of detailed coastal/bottom topography and inflow transport range within which multiple equilibrium path states were achievable. Comprehensive reviews and references on these past studies can be found in Qiu and Miao (2000), Tsujino et al. (2006), and Usui et al. (2013).

The advent of high-precision satellite altimetry measurements in the 1990s provided a new means to explore the Kuroshio path variations from a mesoscale eddy-resolving perspective. As shown in Fig. 1a, two regions with high mesoscale eddy variability outside south of Japan are those in

Corresponding author: Bo Qiu, bo@soest.hawaii.edu

DOI: 10.1175/JPO-D-21-0167.1

© 2021 American Meteorological Society. For information regarding reuse of this content and general copyright information, consult the AMS Copyright Policy ([www.ametsoc.org/PUBSReuseLicenses](http://www.ametsoc.org/PUBSReuseLicenses)).

Brought to you by University of Hawaii at Manoa, Library | Unauthenticated | Downloaded 12/02/21 07:26 PM UTC

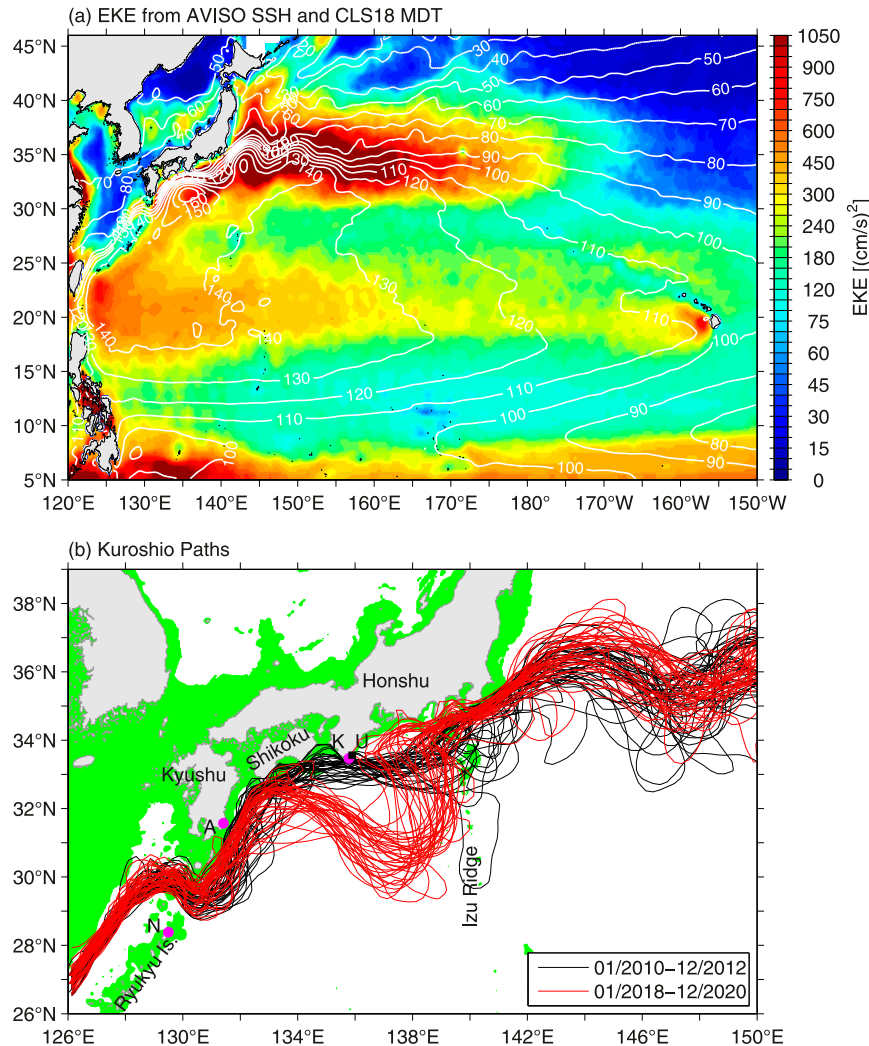


FIG. 1. Eddy kinetic energy (EKE) distribution in the western North Pacific based on the CMEMS satellite altimeter data from 1993 to 2020. White contours denote the mean SSH field by [Rio et al. \(2011\)](#). (b) Monthly Kuroshio paths off Japan during its straight path state in 2010–12 (black lines) vs large-meander state in 2018–20 (red lines). Green shade denotes areas shallower than 500 m. Points N, A, K, and U denote the locations of tide gauge stations Naze, Aburatsu, Kushimoto, and Urugami, respectively.

the STCC band of 18°–28°N east of Taiwan and in the Kuroshio Extension band of 30°–40°N east of the Izu Ridge. In connection to the upstream Kuroshio variability in the East China Sea, several investigators have suggested that anticyclonic eddies originated from the STCC band can modify the Kuroshio transport in the East China Sea and lead to downstream Kuroshio path perturbations south of Japan (e.g., [Akitomo and Kurogi 2001](#); [Ichikawa 2001](#); [Kobashi and Hanawa 2004](#); [Miyazawa et al. 2008](#); [Usui et al. 2008a](#); [Tsujino et al. 2013](#)). In a similar vein, impact by mesoscale eddies emanated from the southern Kuroshio Extension band has also been emphasized by a series of studies (e.g., [Mitsudera et al. 2001](#); [Ebuchi and Hanawa 2003](#); [Miyazawa et al. 2004](#); [Usui et al. 2008b](#)). By translating westward south of 32°N and reaching the Tokara Strait, these mesoscale eddies have been

found to be able to induce perturbations in the Kuroshio path southeast of Kyushu.

It is worth emphasizing that the mesoscale eddies originated from the STCC and the Kuroshio Extension have a time scale of  $O(100)$  days. The frequency of their emergence is, as such, much higher than those of the LM events whose time scales range from interannual to decadal. In order for the mesoscale eddy-induced perturbations to lead to a Kuroshio LM event, additional processes are clearly at work. After a dormant period of 12 years after the last LM event in 2004/05, the Kuroshio path developed into a stable LM state in August 2017 (e.g., [Qiu 2019](#); [Sugimoto et al. 2020](#)). In a recent study to assess the impact of this LM event upon the decadal variability of the Kuroshio Extension dynamic state ([Qiu et al. 2020](#)), we observed that the 2017 LM occurrence was instigated by a

combination of a cyclonic perturbation in Kuroshio path southeast of Kyushu and its subsequent replacement by an intense anticyclonic eddy emanated from the STCC that played critical roles in facilitating the growth of the nascent cyclonic Kuroshio path perturbation, also known as the “trigger meander.”

In light of this new observational evidence of the cyclonic–anticyclonic eddy interaction, we seek in this study to revisit the dynamic processes responsible for the Kuroshio LM occurrences. Questions to be addressed will include 1) how often does the combination of cyclonic–anticyclonic eddy interaction occur off Kyushu, 2) what conditions need to be met for such combination to take place, and 3) to what extent can we understand the occurrence of the past Kuroshio LM events in terms of the cyclonic–anticyclonic eddy interaction versus changes in the upstream Kuroshio transport and in the downstream Kuroshio Extension dynamic state?

This paper is organized as follows. After describing the various datasets in [section 2](#), we review in [section 3](#) definitions for the Kuroshio LM and identify eight LM events in 1950–2020 that form the basis for our analyses. [Section 4](#) quantifies the dependence of LM occurrence on changes in the inflow Kuroshio transport and in the Kuroshio Extension dynamic state. In [section 5](#), mesoscale eddy variations in the STCC band are examined with a focus on eddy’s roles in leading to the 2004/05 LM event. In [section 6](#) we explore the condition conducive to the cyclonic–anticyclonic eddy interactions southeast of Kyushu and relate this condition to the occurrence of the past LM events. [Section 7](#) summarizes the findings from the present study and provides discussion.

## 2. Observational datasets

Long-term sea level data at several tide gauge stations are used in this study to infer the Kuroshio transport and path variations. For the sea level data at Kushimoto (33.48°N, 135.77°E) and Uragami (33.56°N, 135.90°E) (see [Fig. 1b](#) for their locations), we use the monthly product archived by Japan Meteorological Agency (JMA). For the sea level data at Naze (28.38°N, 129.50°E) and Aburatsu (31.58°N, 131.41°E), we utilize the monthly product compiled by the Permanent Service for Mean Sea Level (PSMSL). Concurrent sea level data available for Kushimoto and Uragami started from January 1950 and those for Naze and Aburatsu initiated from March 1961.

To hindcast the long-term dynamic state variability in the downstream Kuroshio Extension region, we utilize the global temperature/salinity (*T/S*) data compiled by JMA Meteorological Research Institute ([Ishii et al. 2017](#)). The monthly *T/S* data are available from 1955 to present and have a 1° horizontal grid resolution in the global 0–3000 m upper ocean.

To examine the surface circulation and eddy variability, we use the global sea surface height (SSH) dataset processed by Ssalto/Duacs and distributed by the Copernicus Marine and Environment Monitoring Service (CMEMS). This dataset merges along-track SSH measurements from all satellite altimeter missions after 1993 and has a 1-day temporal resolution and a 1/4° spatial resolution. The data period analyzed in this study extends from January 1993 to December 2020.

To evaluate transport values associated with the STCC mesoscale eddies, we utilize the conductivity–temperature–depth (CTD) surveys south of Japan conducted by two JMA cruises on 12–25 May and 22–25 July 2004. As will be detailed in [section 5](#), these two cruises traversed several STCC eddies prior to the 2014 LM event. The CTD data have a horizontal resolution of <50 km and a vertical resolution of 1 dbar in the 2000-m upper ocean.

Finally, to relate the oceanic variability to those at the air–sea interface, we adopt the daily data from the European Centre for Medium-Range Weather Forecasts (ECMWF) ERA-5 re-analysis product. The ECMWF ERA-5 data have a spatial resolution of 0.25° and are available from January 1950 to present.

## 3. Kuroshio path indices

Several indices have been used in the past to quantify the Kuroshio path variations south of Japan. An early and long-standing index is that of the tide gauge sea level difference between Kushimoto and Uragami (e.g., [Moriyasu 1961](#); [Kawabe 1980, 1995](#)). Despite the short distance of 14 km separating these two stations, Kushimoto is located at the southern tip of the Kii Peninsula, while Uragami resides in the lee of the peninsula ([Fig. 1b](#)). When it flows closely along the southern coast of Japan, the approaching Kuroshio induces a higher sea level at the tip of the Kii Peninsula than in the lee of the peninsula. This sea level difference, on the other hand, disappears when the Kuroshio takes an offshore meandering path. [Figure 2a](#) shows the time series of sea level difference between Kushimoto and Uragami in the past 70 years. The Kuroshio large meander events, corresponding to periods of diminished sea level difference, can be seen to occur irregularly whose durations can range from slightly longer than 1 year to shorter than 5 years. As noted previously by [Kawabe \(1995\)](#), switching from a straight to LM path, or from a large to small sea level difference state, occurs swiftly, whereas the transition from a meandering and straight Kuroshio path often takes place on time scales of several months.

To characterize the Kuroshio path variations over a broader region, [Qiu and Miao \(2000\)](#) utilized historical hydrographic survey results and defined the Kuroshio path index to be the mean distance of the Kuroshio axis from the southern coast of Japan between 132° and 140°E. In their study, the Kuroshio axis was inferred from the 16°C isotherms at 200-m depth and their derived Kuroshio path index is shown by the dashed line in [Fig. 2b](#). Over their overlapping period, the correlation coefficient between the Kuroshio path index and the time series of Kushimoto–Uragami sea level difference is  $R = 0.75$ . By taking advantage that a Kuroshio LM often involves an intense, onshore cold-core eddy centered at 32°N and 137°E, [Maximenko \(2002\)](#) inferred the past Kuroshio LM events by a linear regression analysis on the three-dimensional water temperature data available after 1930s. As shown by the solid line in [Fig. 2b](#), the LM index time series constructed by [Maximenko \(2002\)](#) agrees favorably with the sea level–based LM variations shown in [Fig. 2a](#) ( $R = -0.74$ ), as well as the offshore distance-based index by Qiu and Miao ( $R = -0.84$ ).

A fourth index that is used widely in recent years to define the Kuroshio LM events is the southernmost latitude of the

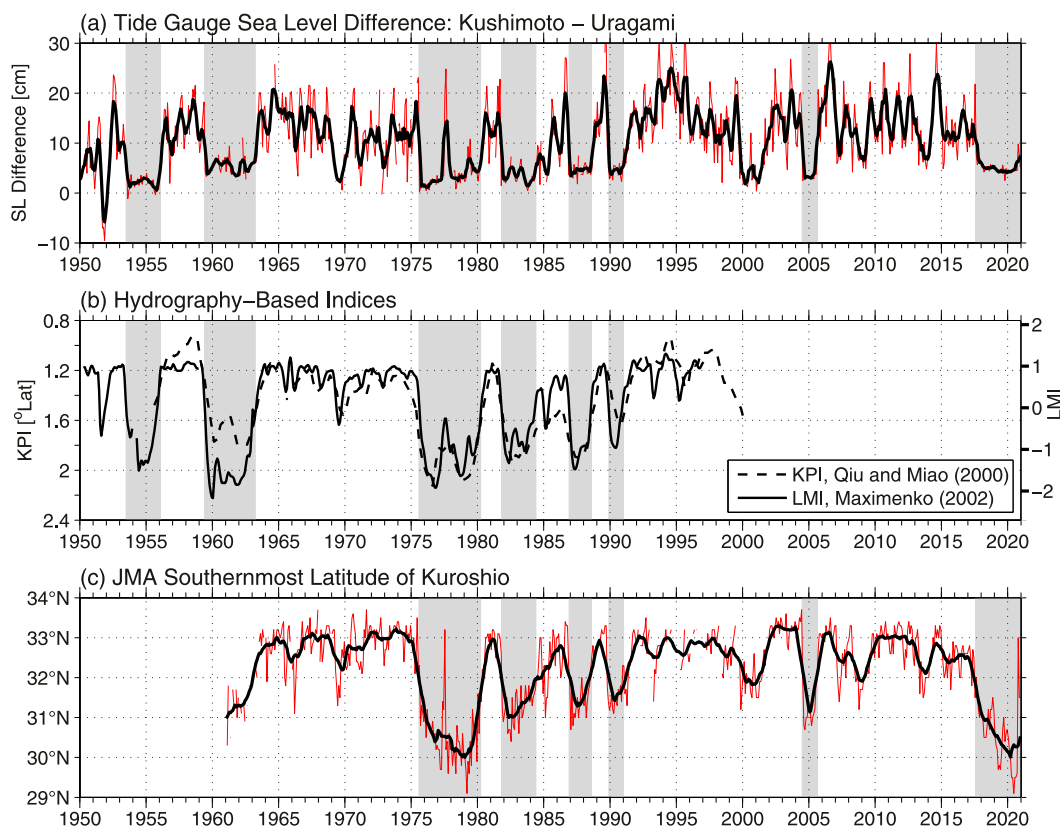


FIG. 2. Time series of (a) sea level difference between the Kushimoto and Urugami tide gauge stations, (b) Kuroshio large meander indices determined by Qiu and Miao (2000; dashed line) and by Maximenko (2002; solid line), and (c) Kuroshio's southernmost latitude south of Japan in the 136°–140°E segment. Red thin lines in (a) and (c) denote the original monthly data, and black lines show the time series after a 13-month running-mean average. Shaded windows denote the eight large meander periods of the Kuroshio analyzed in this study.

Kuroshio path in the 136°–140°E segment based on hydrographic measurements south of Japan (Fig. 2c). Proposed originally by Yoshida et al. (2006), this index is straightforward to construct and has since been adopted by JMA. Specifically, JMA now defines a Kuroshio LM event when this latitudinal index falls below 31.8°N for a consecutive 5-month period ([https://www.data.jma.go.jp/kaiyou/data/shindan/b\\_2/kuroshio\\_stream/kuroshio\\_stream.html](https://www.data.jma.go.jp/kaiyou/data/shindan/b_2/kuroshio_stream/kuroshio_stream.html)). The correlation coefficient between Figs. 2a and 2c is  $R = 0.71$ .

In short, while the various indices presented in Fig. 2 emphasized different aspects of the LM paths, their time series are by and large mutually consistent. This renders defining the Kuroshio LM events straightforward. In Table 1, we list the eight LM events after 1950 with their starting/ending dates and durations. These LM events are also demarcated by gray shades in Fig. 2 and will form the basis for our following statistical analyses. Notice that the dates for LM events 3–8 in Table 1 are the same as those defined by JMA and those for LM events 1–2 are judged based on the time series shown in Figs. 2a and 2b.

#### 4. Upstream and downstream Kuroshio influences

As reviewed in the introduction, many past studies have related the occurrence of the Kuroshio LMs to either the

perturbations originated in the upstream Kuroshio in the East China Sea or those preconditioned by the Kuroshio Extension dynamic state in the downstream Kuroshio region. Given the eight LM events identified in Table 1, we reexamine in this section impacts by the upstream and downstream flow conditions to the occurrence of the past LM events.

The Kuroshio, as depicted in Fig. 1b, exits the East China Sea and enters the deep Shikoku Basin through the narrow Tokara Strait south of Kyushu. From geostrophy, this implies that changes in the Kuroshio transport from the upstream East China

TABLE 1. Starting/ending dates and durations of the Kuroshio large meander events from 1950 to present.

Event No.	Starting/ending dates	Duration (months)
1	Jul 1953–Jan 1956	31
2	Jun 1959–Mar 1963	45
3	Aug 1975–Mar 1980	56
4	Nov 1981–Jul 1984	31
5	Dec 1986–Jul 1988	20
6	Dec 1989–Dec 1990	13
7	Jul 2004–Aug 2005	14
8	Aug 2017–present	>51

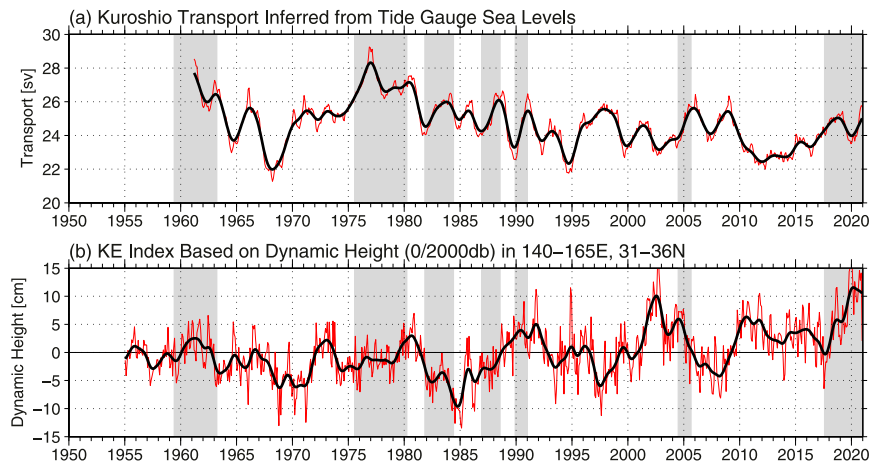


FIG. 3. (a) Time series of the Kuroshio transport through the Tokara Strait inferred from the monthly tide gauge data at Naze and Aburatsu. (b) Time series of the Kuroshio Extension index based on surface dynamic height data in the recirculation gyre box of  $31^{\circ}$ – $36^{\circ}$ N,  $140^{\circ}$ – $165^{\circ}$ E. The long-term mean value is removed. In both plots, red lines denote the original monthly data, and black lines the low-pass-filtered time series retaining interannual and longer time scale signals. Shaded windows denote the large meander periods of the Kuroshio analyzed in this study.

Sea are deducible from tide gauge sea level data across the Tokara Strait. Kawabe (1995) combined seasonal hydrographic surveys in the East China Sea and monthly sea level data across the Tokara Strait and derived several expressions that related the Kuroshio transport changes to the Tokara Strait sea level data through least squares fitting. One such expression is

$$Z_D = 0.326 X_1 - 0.296 X_4 + 24.7, \quad (1)$$

where  $Z_D$  is the Kuroshio transport (Sv), and  $X_1$  and  $X_4$  denote the monthly, 1-yr running-mean, sea level data in centimeters from Naze and Aburatsu, respectively.

Using this expression, we plot in Fig. 3a the Kuroshio transport time series inferred from the Naze and Aburatsu sea level data available after March 1961. The time series reveals that the Kuroshio transport variability in the Tokara Strait has an amplitude of  $\pm 3.5$  Sv and that it changes on both interannual and longer time scales. The fact that a larger transport was observed in the early 1960s and mid- to late 1970s during the LM event 2 and 3 had a significant impact on the earlier studies that explored mechanisms behind the Kuroshio LMs. Indeed, many modeling studies have considered a large inflow Kuroshio transport from the East China Sea to be a prerequisite for the occurrence of LMs (e.g., Chao 1984; Yoon and Yasuda 1987; Akitomo et al. 1996). From the longer time series shown in Fig. 3a, however, the inflow Kuroshio transport does not appear to show an increased tendency prior to the LM occurrences after the 1980s.

To compare and quantify the Kuroshio transport changes in the Tokara Strait preceding/following different LM events, we superimpose in Fig. 4a the Kuroshio transport anomaly time series as a function of starting month for LM events 3–8. Composited over these six events, there do not appear to be a consistent Kuroshio transport change in the Tokara Strait in the 2-yr period prior to the

LM occurrences: the overall Kuroshio transport fluctuated around its time-mean value 24.7 Sv and three LM events experienced inflow accelerations while three other events underwent decelerations. Once a LM takes place, Fig. 4a reveals that there is a tendency for the Kuroshio transport in the Tokara Strait to increase progressively. On average, this increase has a rate of  $\sim 2$  Sv over a period of 15 months. Using the Sverdrup transport values, Usui et al. (2013) have found a similar trend that the upstream Kuroshio transport tended to increase during the LM years.

Availability of the satellite altimetry data after 1993 helps to examine the cause behind the Kuroshio transport changes in the Tokara Strait from a large-scale perspective. To do so, we plot in Fig. 5 monthly SSH anomaly maps regressed to the Kuroshio transport time series shown in Fig. 3a from 1993 to 2020 at different lead times. At zero lead, an enhanced Kuroshio transport is seen in Fig. 5 to be related to a positive SSH anomaly (see the black line) at the northern tip of the Ryukyu Island chain south of the Tokara Strait. As the lead time lengthens, this positive SSH anomaly shows up progressively southward along the Ryukyu Islands and at the 12-month lead, it is seen to be located east of Taiwan in the STCC band of  $20^{\circ}$ – $24^{\circ}$ N. As the lead time lengthens further, the positive SSH anomaly can be traced eastward along the STCC band. In other words, the interannual Kuroshio variability in the East China Sea and the Tokara Strait has its origins in the southern STCC region. This result is in accordance with the findings by Ichikawa (2001), Andres et al. (2008), Chang and Oey (2011), and Hsin et al. (2013) who have respectively identified the Kuroshio variability in the East China Sea to be externally forced by changes originated in the STCC region. Although impactful to the upstream Kuroshio transport fluctuations, our composite result of Fig. 4a indicates that the STCC-induced Kuroshio transport variability via the East China Sea does not play a dominant role in controlling the LM occurrences south of Japan.

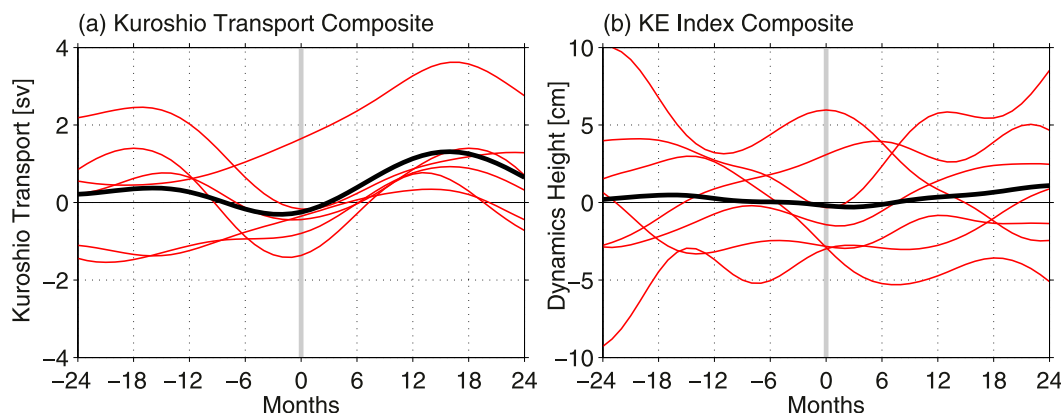


FIG. 4. (a) Composite Kuroshio transport time series through the Tokara Strait (cf. Fig. 3a) as a function of starting month for the LM events 3–8. Red lines denote the changes from individual events, and black line denotes the event averages. (b) As in (a), but for the Kuroshio Extension index time series (cf. Fig. 3b) and for the LM events 2–8.

The Kuroshio Extension southeast of Japan is known to experience decadal oscillations between a stable and an unstable dynamic state (e.g., Qiu and Chen 2005, 2010a; Taguchi et al. 2007). During its stable state, the upstream Kuroshio Extension jet migrates northward, forcing its entry path into the open North Pacific across 140°E to lean against the Japanese coast. During its unstable state, the upstream Kuroshio Extension jet tends to shift southward, overriding the shallow Izu Ridge that parallels 140°E. As shown in

Fig. 1b, a stable Kuroshio Extension dynamic state, with its entry path anchored against the Japanese coast, has been considered to favor the LM occurrence (Usui et al. 2013).

Variations in the Kuroshio Extension dynamic state can be reliably represented by the SSH values in its southern recirculation region of 31°–36°N and 140°–165°E (Qiu et al. 2014). Specifically, higher-than-normal SSH values are observed in a stable dynamic state due to strengthening of the Kuroshio Extension recirculation. To quantify the time-varying Kuroshio Extension dynamic state in

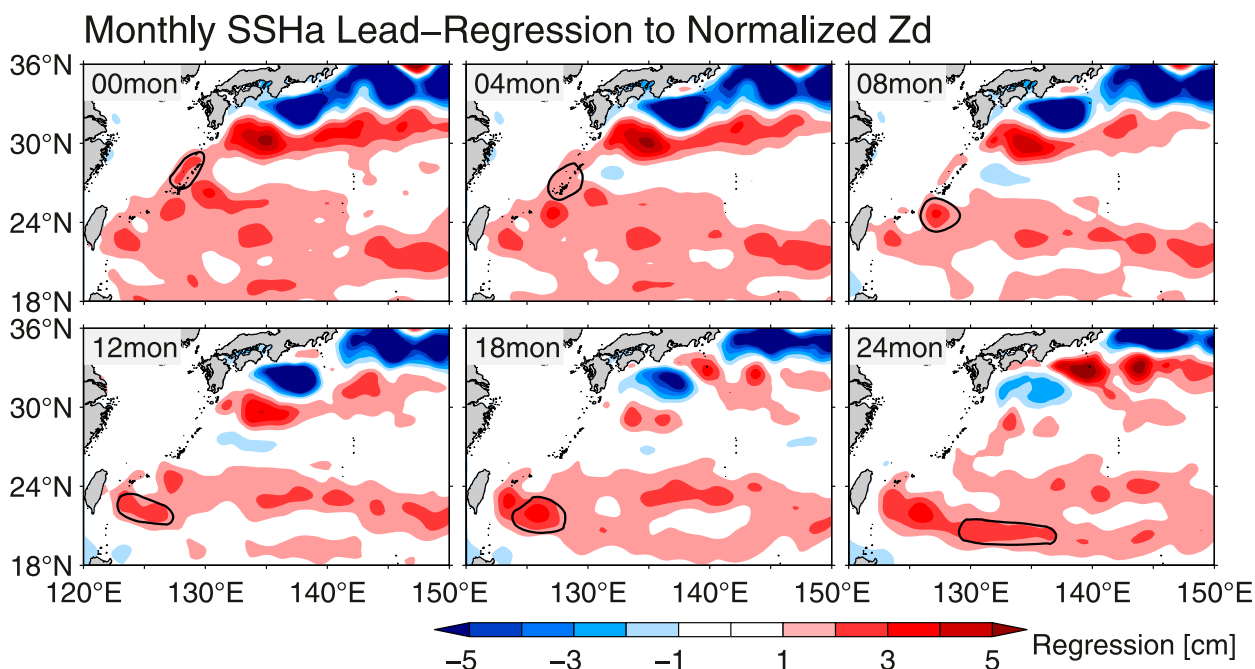


FIG. 5. Monthly SSH anomaly maps regressed to the normalized Kuroshio transport time series across the Tokara Strait from 1993 to 2020 (Fig. 3a) at different lead times. Here, lead time is denoted in the upper left of each map and the SSH anomaly data are based on the CMEMS product with the  $3.2 \text{ mm yr}^{-1}$  global-mean sea level trend removed. Black lines denote the evolution of the positive SSH anomaly responsible for the Kuroshio transport change across the Tokara Strait.

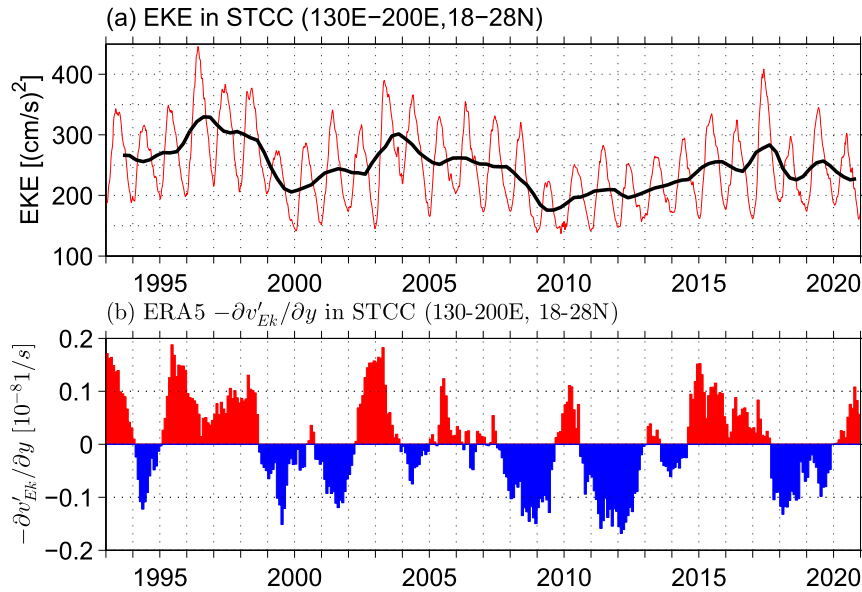


FIG. 6. (a) EKE time series in the STCC band of 18°–28°N, 130°–200°E. The red line shows the weekly time series and black line the low-pass-filtered time series retaining interannual and longer time scale signals. (b) Time series of meridional Ekman flux convergence anomalies in the STCC band after removal of the climatological seasonal cycle.

the past 70 years, we use the globally gridded  $T/S$  data from 1955 compiled by Ishii et al. (2017) and calculate the surface dynamic height time series referenced to 2000 dbar in the 31°–36°N and 140°–165°E region of our interest (Fig. 3b). In agreement with the past studies based on other available data sources (e.g., Qiu et al. 2014; Na et al. 2018; Joh and Di Lorenzo 2019), Fig. 3b reveals that the Kuroshio Extension dynamic state underwent vigorous decadal modulations and this is particularly true after the 1976/77 climate regime shift in the North Pacific.

To relate the Kuroshio Extension dynamic state changes to the LM occurrences, we plot in Fig. 4b the surface dynamic height anomaly time series as a function of starting month for LM events 2–8. The connection between the two appears highly variable. LM events 6 and 7 started when the Kuroshio Extension was in a stable dynamic state and LM events 3 and 5 occurred while the Kuroshio Extension dynamic state was unstable. Three other LM events took place when the Kuroshio Extension was in transition periods between stable and unstable states. Because of these diverse conditions, the seven-event composite in Fig. 4b reveals no clear dependence by LM occurrences on the Kuroshio Extension dynamic state. Instead of being affected by the Kuroshio Extension dynamic state, our recent study indicated that for the recent LM event 8, it is in fact the LM occurrence in August 2017 that reversed the Kuroshio Extension from its preexisting wind-forced unstable state to a LM-driven stable state (Qiu et al. 2020).

## 5. STCC mesoscale eddy variations

Given the weak connections between the LM occurrences and the up/downstream Kuroshio variability detailed above, we explore in this section the extent to which the LM occurrences may

be instigated by mesoscale eddy variations from the STCC region of 18°–28°N. Despite being a shallow and relatively weak mean eastward current with a speed of  $O(5) \text{ cm s}^{-1}$ , the STCC, as shown in Fig. 1a, exhibits enhanced mesoscale eddy variability as a result of baroclinic instability involving the surface eastward-flowing STCC and subsurface westward-flowing NEC (Qiu 1999; Kobashi and Kawamura 2002; Noh et al. 2007). Notice that the time-mean STCC has three branches and, as it moves eastward, the mean position of the STCC shifts northward (Kobashi et al. 2006). Accompanying this poleward shift, the high EKE band of the STCC also migrates northward.

To explore the relevance of STCC eddies upon the LM occurrence, it is helpful to focus first on the satellite altimetry period after 1993 when altimetry SSH measurements captured fully the oceanic mesoscale eddy field. Figure 6a shows the SSH-derived eddy kinetic energy (EKE) time series in the STCC band of 18°–28°N, 130°–200°E. Prominent seasonal and interannual variations are clearly existent with the seasonal EKE level peaking in May–June and eddy-rich years appearing in 1996–98, 2003–08, and 2015–17, respectively. Dynamically, the STCC band EKE level is determined by the strength of baroclinic instability, or the vertical zonal velocity shear between STCC and NEC,  $\partial U_g/\partial z$ . From the thermal wind balance, this vertical zonal velocity shear is related to the meridional upper-ocean temperature gradient  $\partial T/\partial y$  via  $f\partial U_g/\partial z = -\alpha g\partial T/\partial y$ , where  $f$  is the Coriolis parameter,  $g$  is the gravity constant, and  $\alpha$  is the thermal expansion coefficient. Because the upper-ocean temperature variations around the center of the wind-driven subtropical gyre are largely controlled by meridional Ekman advection, changes in  $\partial U_g/\partial z$  can be approximated by

$$\frac{\partial}{\partial t} \left( \frac{\partial U_g}{\partial z} \right) \simeq \frac{\alpha g}{f} \frac{\partial}{\partial y} \left( v_{Ek} \frac{\partial T}{\partial y} \right), \quad (2)$$

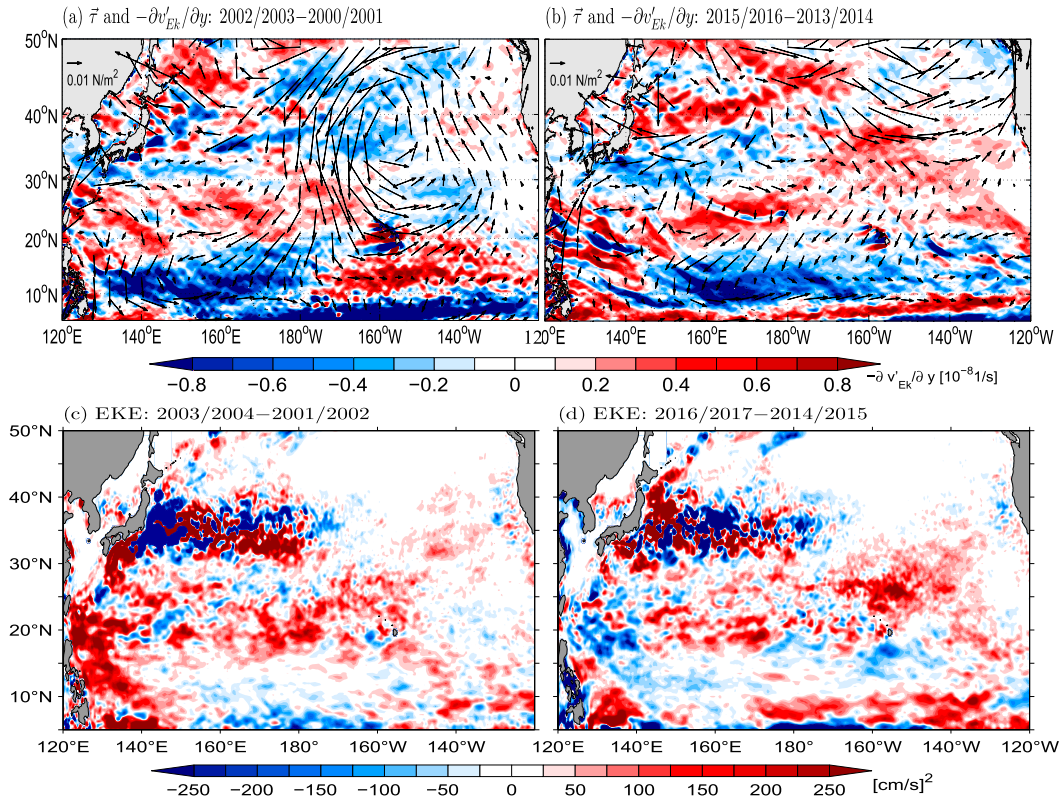


FIG. 7. Difference maps in wind stress vectors and meridional Ekman flux convergence (in color) in the North Pacific Ocean: (a) years 2002/03 – 2000/01 and (b) 2015/16 – 2013/14. (c),(d) As in (a) and (b), but for the altimeter-measured EKE levels with a 1-yr lag.

where  $v_{\text{Ek}} = -\tau^x / (f\rho_0 H_0)$  is the meridional Ekman velocity in the upper ocean,  $\tau^x$  is the zonal wind stress,  $\rho_0$  is the reference density, and  $H_0$  ( $=150$  m) is the upper-ocean thickness. Our previous analysis based on in situ data (section 4 in Qiu and Chen 2010b) indicated that the meridional Ekman advection term on the RHS of (2) can be further simplified to

$$\frac{\partial}{\partial t} \left( \frac{\partial U_g}{\partial z} \right) \simeq \frac{\alpha g}{f} \frac{\partial v'_{\text{Ek}}}{\partial y} \frac{\partial \bar{T}}{\partial y}, \quad (3)$$

where an overbar denotes the time-mean value and prime denotes deviation from the time-mean. Since  $\partial \bar{T} / \partial y < 0$  in the STCC band, Eq. (3) implies that changes in  $\partial U_g / \partial z$  follow those in meridional Ekman flux convergence anomalies: a convergent anomaly (i.e.,  $-\partial v'_{\text{Ek}} / \partial y > 0$ ) strengthens the vertical zonal velocity shear and vice versa.

In Fig. 6b, we plot the time series of  $-\partial v'_{\text{Ek}} / \partial y$  for the satellite altimetry period. To focus on the interannual variability, we have removed its monthly climatology.<sup>1</sup> As indicated in

Eq. (3), periods with enhanced  $-\partial v'_{\text{Ek}} / \partial y$  preceded years when the observed EKE level was elevated. To demonstrate the connections between the convergent Ekman flux forcing and the EKE modulations in the context of LM occurrence, we plot in Figs. 7a and 7b the difference maps of  $-\partial v'_{\text{Ek}} / \partial y$  between 2002/03 and 2000/01 and between 2015/16 and 2013/14, respectively. For both cases, the meridional Ekman flux convergence anomalies in the first two years are predominantly positive and those in the latter two years, negative. The difference maps reveal that the positive  $-\partial v'_{\text{Ek}} / \partial y$  anomalies in both cases exist coherently across the STCC band and physically, as indicated by the wind stress vectors, they are related to the regional development of anticyclonic surface wind circulations. Figures 7c and 7d show maps of the EKE difference between the years lagging those in Figs. 7a and 7b by one year. In response to the convergent Ekman flux forcings in both cases, mesoscale eddy activities in the STCC band are observed to increase significantly. Compared to the time-mean EKE level of  $250 \text{ cm}^2 \text{ s}^{-2}$  in the STCC band (Fig. 6a), the EKE difference value between the eddy-rich and eddy-poor years can reach a nearly equal magnitude of  $200 \text{ cm}^2 \text{ s}^{-2}$ .

The eddy-rich years of 2003/04 and 2016/17 shown in Figs. 7c and 7d preceded the LM events 7 and 8, respectively. To demonstrate the impact of mesoscale eddies upon the LM occurrence, we show in Fig. 8 the monthly SSH anomaly field leading to the 2004/05 LM event (similar maps can be found in Usui et al.

<sup>1</sup> On the monthly time scale,  $-\partial v'_{\text{Ek}} / \partial y$  peaks in December/January and induces a seasonal  $\partial U_g / \partial z$  maximum in March. The seasonal EKE peak in May seen in Fig. 6a is a result of weak growth of baroclinic instability in the vertically sheared STCC–NEC system (Qiu 1999).

## 09/2003–08/2004 Monthly SSHa

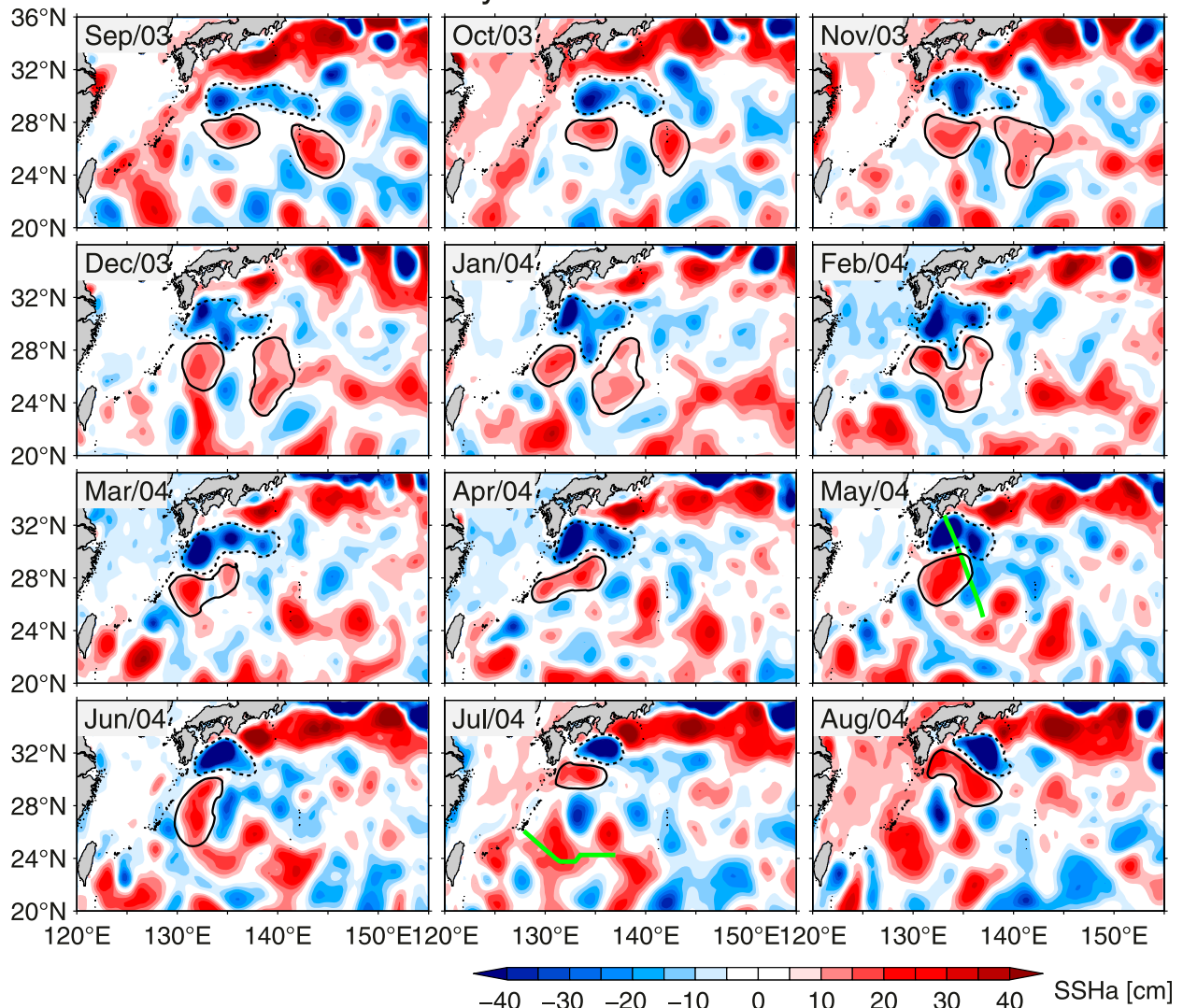


FIG. 8. Monthly maps of SSH anomalies from September 2003 to August 2004 in the western North Pacific Ocean. To avoid large-scale steric height changes due to seasonal heating/cooling, the area mean SSH anomaly value of each month is removed. Dashed lines denote the evolution of the trigger meander that appeared southeast of Kyushu in March 2004 and solid lines, the positive SSH anomalies that replaced the trigger meander off Kyushu in July 2004. Green lines in May/04 and Jul/04 maps denote locations of the JMA cruises NC0404 and NC0406, respectively.

2008a,b). As indicated in the mid-bottom map, the 2004 LM is fully established in July 2004 and its presence corresponds geostrophically to the negative SSH anomaly (the dashed line) south of Japan. Tracking it backward in time, this negative SSH anomaly can be seen to have initiated in the upstream Kuroshio southeast of Kyushu in March 2004 and whose origin can be further traced back to 135°–145°E along 30°N as a sequence of cyclonic mesoscale eddies in the fall 2003. The negative SSH anomaly, such as that appearing off Kyushu in May 2004, is known as “trigger” meander and its role as a precursor to the LM occurrence has been emphasized in many previous studies (e.g., Solomon 1978; Mitsudera et al. 2001; Ebuchi and Hanawa 2003; Miyazawa et al. 2004; Usui et al. 2008a).

Another feature that is of equal importance to the 2004 LM development is an intense *positive* SSH anomaly that emerged southeast off Kyushu in July 2004 (the solid line in mid-bottom map of Fig. 8). This positive SSH anomaly, or anticyclonic eddy, originated about a year ago in the STCC band of 24°–28°N, where a pair of anticyclonic eddies can be seen in Fig. 8 to merge while propagating westward and to migrate northward after impinging upon the Ryukyu Islands. It is worth stressing that this *same* sequence of events, namely, emergence of a trigger meander off Kyushu that was then replaced by an intense anticyclonic eddy, were observed in 2016/17 that led to the 2017 LM event (see Fig. 7 in Qiu et al. 2020).

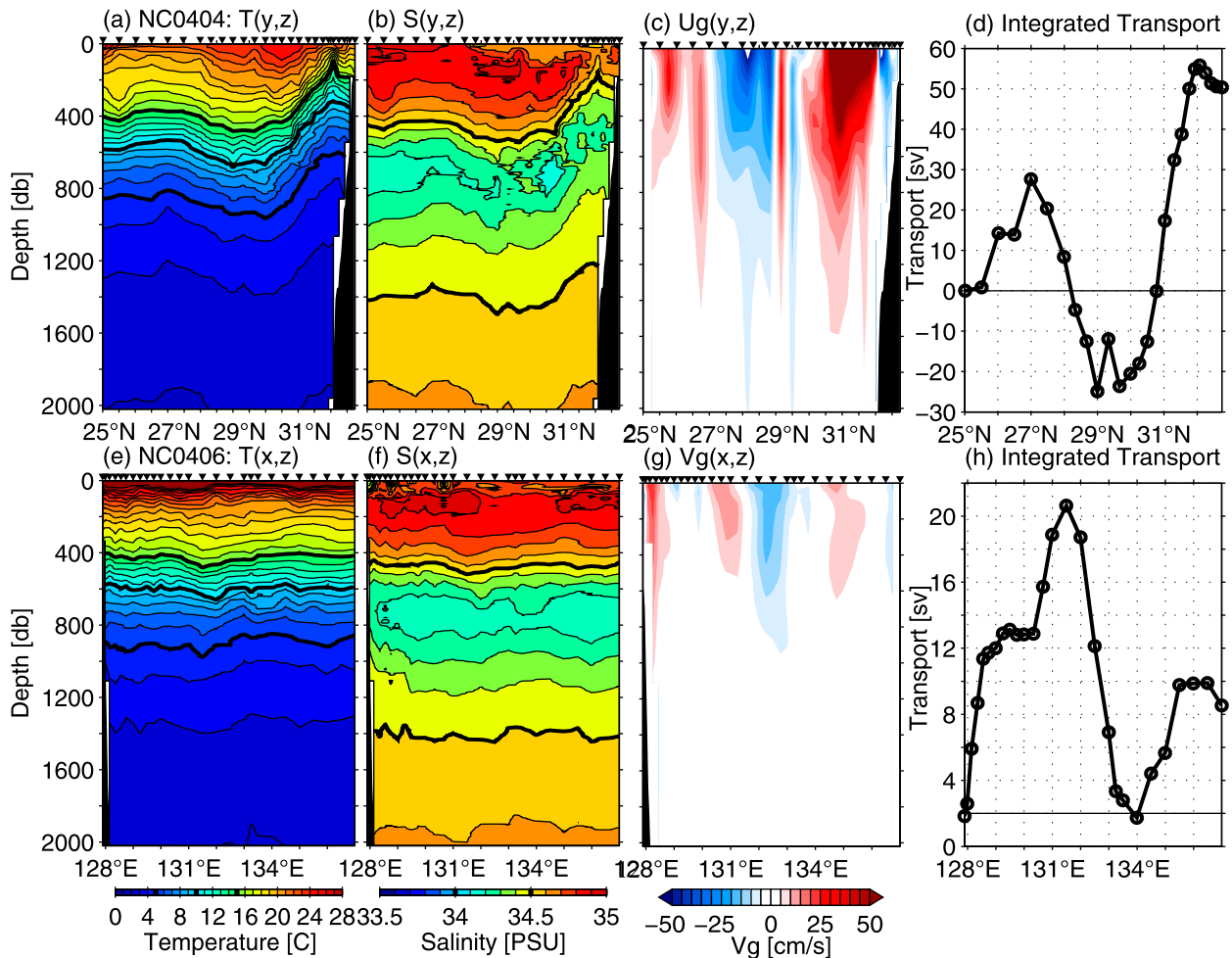


FIG. 9. Cross-section profiles of (a) temperature, (b) salinity, (c) geostrophic velocity (referenced to 6000 dbar), and (d) integrated volume transport from the JMA cruise NC0404 of 5–12 May 2004. See the green line in the May/04 map in Fig. 8 for the section location. (e)–(h) As in (a)–(d), but from the JMA cruise NC0406 of 22–25 July 2004. The reference level for (g) is 2020 dbar, and the section location is shown by green line in the Jul/04 map in Fig. 8.

To assess the properties of anticyclonic eddies originated from the STCC band, we present in Fig. 9 the hydrographic survey results by JMA that transversed two STCC anticyclonic eddies in 2004. As indicated by green line in the May/04 map of Fig. 8, the JMA NC0404 cruise of 5–12 May crisscrossed the cyclonic trigger meander, the Kuroshio jet, and the anticyclonic eddy of our interest south of Shikoku. Figures 9a–c show the cross sections of temperature, salinity, and cross-track (approximately zonal) geostrophic velocity referenced to 6000 dbar. To facilitate transport estimates associated with the eddies and Kuroshio jet, we plot in Fig. 9d the transport values integrated from the southern end of the cruise track. The Kuroshio jet, accompanied by the steep  $T/S$  fronts between 30.8° and 31.8°N, has a net eastward transport of 50 Sv. This net transport value for Kuroshio is consistent with the previous estimate across this section by Imawaki et al. (2001, their Fig. 3b). North of the Kuroshio jet, the transport value associated with the cyclonic trigger meander is estimated at 6 Sv. Due to the presence of bottom slope, the trigger meander is mostly confined to the 1000 dbar upper ocean.

In contrast, the anticyclonic eddy appearing between 28.0° and 30.8°N (see green line in the May/04 map of Fig. 8) has a transport value reaching 25 Sv and, as shown in Figs. 9a and 9b, its downwelling  $T/S$  expressions are observed to extend to deeper than 2000 dbar. Notice that the NC0404 cruise did not traverse across the center of the anticyclonic eddy and, as such, the 25 Sv value could be an underestimate for its true transport.

On 22–25 July 2014, the JMA cruise NC0406 crisscrossed another anticyclonic eddy that appeared in 128°–134°E east of the Ryukyu Islands (see green line in the Jul/04 map of Fig. 8). Although the downwelling  $T/S$  expressions by this anticyclonic eddy appear less deep-reaching (Figs. 9e,f) than those detected in the May cruise,<sup>2</sup> Fig. 9h reveals that this anticyclonic eddy of the STCC has, nevertheless, a transport as large as 21 Sv. It is

<sup>2</sup> The deep  $T/S$  expressions by the anticyclonic eddy captured by the May cruise are likely due to the coalescing of two STCC anticyclonic eddies as we noted earlier from Fig. 8.

worth recalling that the inflow Kuroshio transport fluctuations across the Tokara Strait has an amplitude of 6 Sv (Fig. 3a). With their transport values in excess of 20 Sv, intense anticyclonic eddies originating from the STCC can be expected to exert a greater impact upon the Kuroshio path variations south of Japan.

## 6. Combined processes leading to LM events

Based on the results of the preceding sections, we propose in this study that the combined emergence of a cyclonic meander and a subsequent, intense, anticyclonic eddy southeast of Kyushu is the required process for the occurrence of a LM event. To highlight the importance of this combination, we follow our 2020 study and plot in Fig. 10a the time series of negative SSH anomalies averaged in the 4°-wide band from 29° to 32°N southeast of Kyushu. It is evident from this time series that persistent negative SSH anomalies, or trigger meanders, appeared quite frequently off Kyushu. In other words, a trigger meander is a necessary, but not *sufficient* process for a LM occurrence. For comparison, we plot in Fig. 10b the time series of SSH anomalies averaged in the 4°-wide band from 24° to 29°N east of the Ryukyu Islands. While there exist interannual modulations in the magnitudes of SSH anomalies, no apparent preference for positive SSH anomalies, i.e., anticyclonic eddies, are discernible in Fig. 10b.

To identify the episodes and intensity wherein a trigger meander is succeeded by an anticyclonic eddy from the STCC band, we plot in Fig. 10c the product of the time series of Fig. 10a and that of Fig. 10b with a lag of 4 months. Here, the 4-month lag is chosen to allow mesoscale anomalies to propagate from east of the Ryukyu Islands to southeast of Kyushu. For clarity, only negative product (i.e., a trigger meander followed by an anticyclonic eddy) is shown in Fig. 10c. Episodes with large negative product values were relatively rare; they occurred in late 1998, late 2002, late 2003–early 2004, late 2006, late 2007, and early 2017, respectively. To relate these episodes to the Kuroshio path variations south of Japan, we superimpose on Fig. 10c a black line showing the southernmost latitude of Kuroshio defined in Fig. 2c. Of the six episodes noted above, those of late 2003–early 2004 and early 2017 developed to the two latest LM events listed in Table 1. Although failed to reach the LM status, the remaining episodes, with an exception for the late 2002 episode, have led to offshore excursions by the Kuroshio south of Japan.

A closer look at the late 2002 episode in Figs. 10a and 10b indicates that its large negative product value is caused by a very intense trigger meander, which was followed by a weak anticyclonic eddy east of the Ryukyu Islands. Dynamically, while a trigger meander southeast of Kyushu provides the initial cyclonic perturbation to the Kuroshio path, the successive emergence of an intense anticyclonic eddy off Kyushu plays two critical roles: 1) it prevents the initial cyclonic perturbation from migrating westward due to the planetary  $\beta$  effect (Tsujino et al. 2006), and 2) its presence thrusts the Kuroshio jet northward against the coast of Kyushu/Shikoku, generating positive relative vorticities along the coast that can be advected downstream to strengthen the cyclonic LM path.

In other words, succeeding a trigger meander off Kyushu by an *intense* anticyclonic eddy is an indispensable process for the occurrence of a full-fledged LM event. Indeed, the episodes with large negative product values in Fig. 10c all took place in the years when EKE level in the STCC band was anomalously high (cf. Fig. 6a). This is of no surprise because when the STCC eddy activity level is elevated, there are increased chances for a trigger meander off Kyushu to be succeeded by an intense anticyclonic eddy and lead to a LM occurrence.

To explore the relationship between the STCC eddy activities and the past LM events beyond the satellite altimetry era, we adopt the meridional Ekman flux convergence anomaly,  $-\partial v'_{\text{Ek}}/\partial y$ , as a proxy for the EKE level in the STCC band. As derived in Eq. (3),  $-\partial v'_{\text{Ek}}/\partial y$  controls the evolution of vertical zonal velocity shear and is an energy source for the baroclinically unstable STCC–NEC system. For the two latest LM events, we have shown in Fig. 7 that the positive  $-\partial v'_{\text{Ek}}/\partial y$  anomalies in the STCC band were indeed accompanied by enhanced regional eddy activities. Figure 11a shows the time series of meridional Ekman flux convergence anomalies in the STCC band based on the ERA5 wind stress product. With an exception for the 1990 LM event, it can be seen that the seven other LM events *all* occurred following several years of convergent meridional Ekman flux anomalies.

In Fig. 12, we superimpose the meridional Ekman flux convergence time series as a function of starting month for all eight LM events. In the 3-yr period preceding the LM occurrence, the composite  $-\partial v'_{\text{Ek}}/\partial y$  is positive and has a maximum value appearing 12–24 months prior to the LM events. Physically, this 12–24-month lead represents the time required for the convergent meridional Ekman flux forcing to strengthen the vertical zonal velocity shear, the time for the baroclinic instability to grow and produce finite-amplitude eddies, and the time for intense anticyclonic eddies to reach southeast of Kyushu. The composite result of Fig. 12, thus, supports our hypothesis that LM events are favored to take place when mesoscale eddy activities in the STCC are enhanced, so that cyclonic trigger meanders off Kyushu have an increased chance to be succeeded by intense anticyclonic eddies originated from the STCC band.

## 7. Summary and discussion

By synthesizing the in situ observational data (i.e., tide gauge sea level, hydrographic surveys, and gridded  $T/S$  product), surface wind stress reanalysis, and satellite altimetry measurements, we have in this study reassessed the dynamic processes that are inductive to the occurrence of the Kuroshio LMs south of Japan. Although different methodologies have been proposed in the past to identify the LM event, we found that these methods are mutually consistent and that the existing LM events can be robustly defined. A total of eight LM events have occurred from 1950 to 2020, and these eight LM events formed the basis for our analyses.

Previous studies on the Kuroshio path modality have sought causes in the inflow Kuroshio transport changes from the East China Sea. The longer records available now provide us an opportunity to reexamine the relationship between the LM occurrence and the upstream Kuroshio transport changes. By

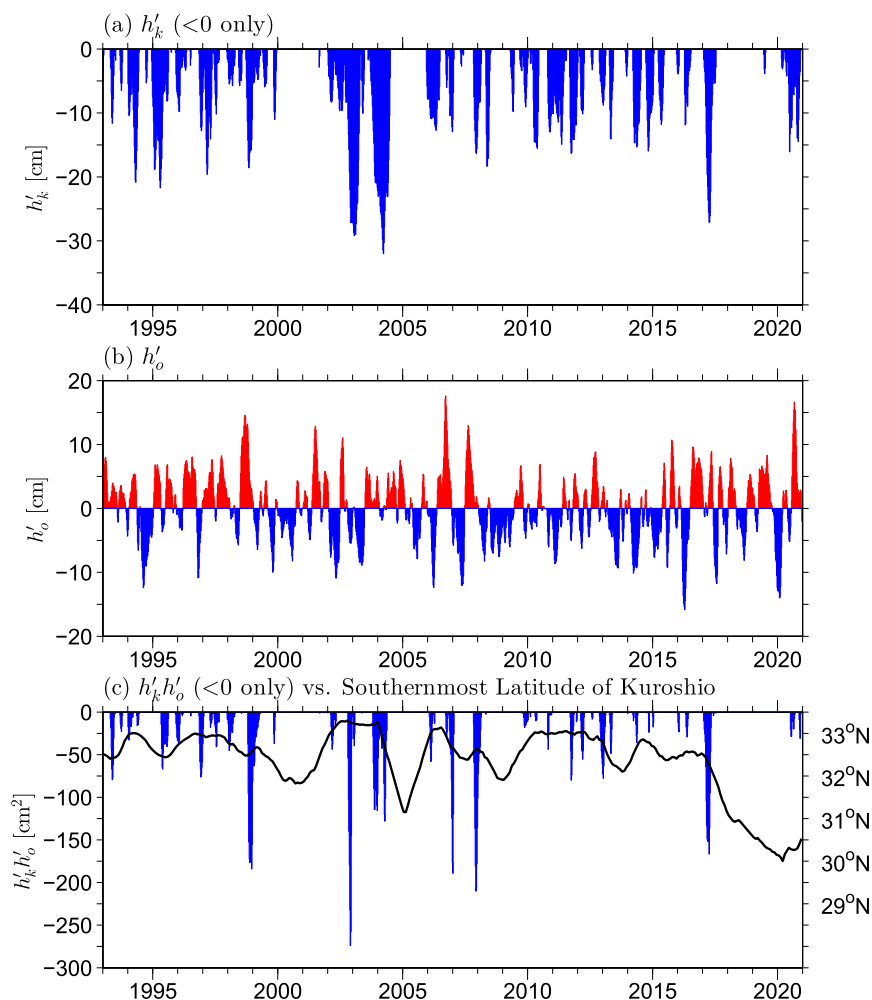


FIG. 10. (a) Time series of SSH anomalies averaged in a  $4^\circ$  longitude-wide band from  $29^\circ$  to  $32^\circ$ N southeast of Kyushu. Only negative anomalies denoting the Kuroshio trigger meanders are shown. (b) Time series of SSH anomalies averaged in the  $4^\circ$  longitude-wide band east of the Ryukyu Islands from  $24^\circ$  to  $29^\circ$ N. (c) Product of the SSH anomalies shown in (a) and (b) with a lag of 4 months. Only negative anomalies denoting trigger meanders followed by positive SSH anomalies east the Ryukyu Islands are shown. Black line denotes Kuroshio's southernmost latitude defined in Fig. 2c.

utilizing the tide gauge sea level data across the Tokara Strait as a proxy for the inflow Kuroshio transport, we found no consistent inflow transport changes among the six LM events in the 1961–2020 period of sea level data availability. The Kuroshio transport changes across the Tokara Strait have an amplitude of  $\pm 3$  Sv. With the net eastward transport of the Kuroshio south of Japan reaching 50 Sv, this level of inflow transport changes might be too small to bring about the Kuroshio path fluctuations to reach the amplitude of a LM.

By influencing Kuroshio's outflow condition over the shallow Izu Ridge, low-frequency modulations in the downstream Kuroshio Extension dynamic state have also been considered to possibly affect the Kuroshio path south of Japan. To explore this possibility, we constructed a long-term proxy representing the Kuroshio Extension dynamic state based on the gridded  $T/S$  product of Ishii et al. (2017). Similar to the inflow Kuroshio transport changes, no

clear connection was detected between the LM occurrences and the Kuroshio Extension dynamic state changes.

Instead of the upstream and downstream influences from the Kuroshio itself, our present study advocated the roles played by mesoscale eddies originated from the STCC in initiating a LM event. Specifically, we proposed that the interaction between a cyclonic trigger meander off Kyushu and a succeeding, intense, anticyclonic eddy of the STCC origin, forms an inductive condition for the LM occurrence. Evidence for such interaction leading to the 2004/05 LM event was presented in this study and a similar interaction that initiated the 2017 LM was given in Qiu et al. (2020). It is worth emphasizing that the typical transport associated with a well-developed STCC anticyclonic eddy is in excess of 20 Sv. These intense eddies can interact with the Kuroshio jet effectively by anchoring cyclonic trigger meanders to the east and by

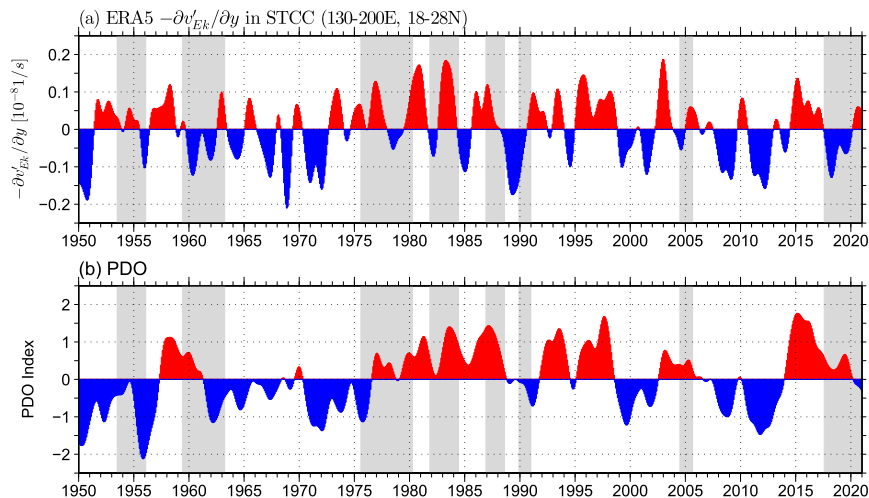


FIG. 11. (a) Time series of meridional Ekman flux convergence anomalies in the STCC band. (b) Time series of the Pacific decadal oscillation (PDO) index. For both time series, signals with time scales shorter than 1.5 years have been removed.

supplying positive relative vorticity from coast to strengthen the nascent cyclonic meander path.

Our analysis of the satellite altimetry data of 1993–2020 revealed that the episodes of a cyclonic trigger meander to be succeeded by an intense anticyclonic eddy southeast of Kyushu happened infrequently. A favorable condition for its happening is when the surface wind stress forcing over the STCC band is anomalously anticyclonic. Such anticyclonic wind stress forcing induces convergent meridional Ekman fluxes, strengthens the vertical STCC–NEC shear, and produces more intense meso-scale eddies that have a chance to succeed the trigger meanders off Kyushu. As is evident from Fig. 1a, the presence of the Ryukyu Islands in this case plays the role of a lateral boundary that propels approaching anticyclonic STCC eddies poleward through their image effect (e.g., Kundu et al. 2016, section 5.6) to reach the southeast of Kyushu.

Building on the insights gleaned from the satellite altimetry data, we examined the past LM events in connection to the meridional Ekman flux convergence forcing in the STCC band from 1950 to 2020. Out of the eight LM events in the past 70 years, seven LM events are found to be preceded by years of convergent meridional Ekman flux forcing, consistent with our hypothesis that the LM occurrence is favored when the wind-forced STCC eddy variability is enhanced. The one LM event which did not follow a convergent meridional Ekman flux forcing took place in December 1989–December 1990 (Fig. 11a). As this LM event preceded the satellite altimetry era, it is unclear what exact processes led to its occurrence. Given the short time separation between it and the prior 1987/88 LM event, it is possible that the processes responsible for the 1990 LM event may be different from those involving trigger meanders and intense anticyclonic eddies from the STCC band. It will be of interest for future studies to unravel the processes behind this “unusual” LM event.

In contrast to the 1990 LM event that followed no convergent meridional Ekman flux forcing, Fig. 11a reveals that

convergent meridional Ekman flux anomalies persisted from 1995 to 1998, but failed to lead to a LM occurrence. A close inspection of Figs. 2a and 2c indicates that although not designated to be a formal LM event, the Kuroshio path did take a significant southward detour from late 1999 to mid-2001. Furthermore, Fig. 10c shows that this southward detour by the Kuroshio was initiated by the combined emergence of a trigger meander and a subsequent intense anticyclonic eddy southeast of Kyushu. It is worth emphasizing the threshold for defining a LM event was chosen subjectively by JMA. Relaxing the southernmost Kuroshio latitude threshold from  $31.8^{\circ}$  to  $32^{\circ}\text{N}$  would have designated the offshore detouring Kuroshio path from January 2000 to March 2001 to be a LM event.

In closing, we note that the surface wind variability that generated the meridional Ekman flux convergence

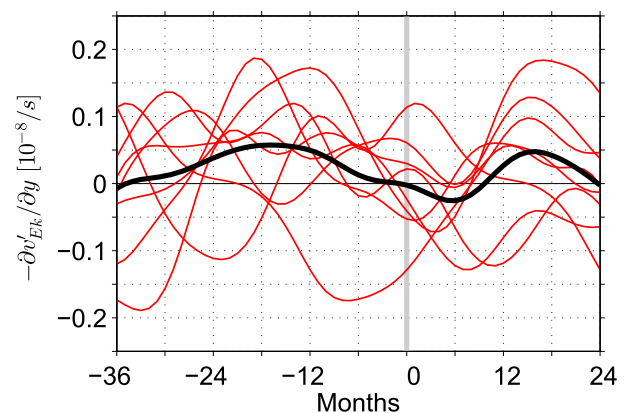


FIG. 12. Composite meridional Ekman flux convergence anomaly time series (cf. Fig. 11a) as a function of starting month of the eight LM events listed in Table 1. Red lines denote the time series from individual events, and the black line denotes the event averages.

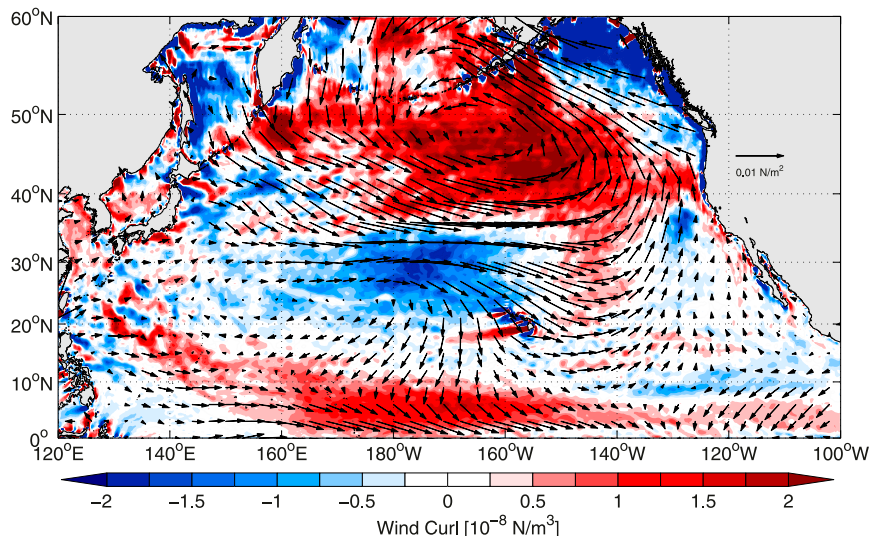


FIG. 13. Surface wind stress vector and curl (in color) regressed to the normalized PDO index of 1950–2020 shown in Fig. 11b.

anomalies shown in Fig. 11a is *not* a local phenomenon confined to the subtropical western North Pacific. In Fig. 11b we plot the Pacific decadal oscillation (PDO) index that represents the broadscale climate variability in the entire North Pacific basin (Mantua et al. 1997). There exists a favorable correlation between the PDO index and Fig. 11a with their correlation coefficient  $r$  reaching 0.52 (with the number of degrees of freedom in the two time series estimated to be 25, this  $r$  value exceeds the 99% confidence level). The reason behind this favorable correlation is that despite being dominated by the Aleutian low variability over the midlatitude North Pacific, the PDO surface wind variability has a large-amplitude imprint over the subtropical western North Pacific Ocean (Fig. 13). Specifically, in its positive phasing, the PDO surface wind exhibits an anticyclonic anomaly over the STCC band that works to enhance the convergent meridional Ekman flux forcing and elevate the regional mesoscale eddy activities (recall Fig. 7). Given this connection to the PDO forcing, it is important for future studies to explore the Kuroshio path variations in the context of the broadscale climate variability in the North Pacific basin.

**Acknowledgments.** Constructive comments made by two anonymous reviewers have improved an early version of the manuscript. The ECMWF ERA-5 reanalysis data used in this study were accessed from <https://cds.climate.copernicus.eu/>, the JMA tide gauge data from [https://www.data.jma.go.jp/gmd/kaiyou/db/tide/sea\\_leve\\_var/index\\_history.php](https://www.data.jma.go.jp/gmd/kaiyou/db/tide/sea_leve_var/index_history.php), the JMA hydrographic cruise data and analysis information from [https://www.data.jma.go.jp/gmd/kaiyou/db/vessel\\_obs/data-report/html/ship/ship.php](https://www.data.jma.go.jp/gmd/kaiyou/db/vessel_obs/data-report/html/ship/ship.php), the PSMSL tide gauge data from <http://www.psmsl.org>, the MRI T/S data from <https://climate.mri-jma.go.jp/pub/ocean/ts/v7.3/>, and the merged satellite altimeter data from Ssalto/Duacs and the Copernicus Marine and Environment Monitoring Service (<http://www.marine.copernicus.eu>). We ac-

knowledge the support of NSF Grant 2019312 and NASA Grant NNX17AH33G.

#### REFERENCES

- Akitomo, K., and M. Kurogi, 2001: Path transition of the Kuroshio due to mesoscale eddies: A two-layer, wind-driven experiment. *J. Oceanogr.*, **57**, 735–741, <https://doi.org/10.1023/A:1021292627245>.
- , M. Ooi, and T. Awaji, 1996: Interannual variability of the Kuroshio transport in response to the wind stress field over the North Pacific: Its relation to the path variation south of Japan. *J. Geophys. Res.*, **101**, 14 057–14 071, <https://doi.org/10.1029/96JC01000>.
- Andres, M., M. Wimbush, J.-H. Park, K.-I. Chang, B.-H. Lim, D. R. Watts, H. Ichikawa, and W. J. Teague, 2008: Observations of Kuroshio flow variations in the East China Sea. *J. Geophys. Res.*, **113**, C05013, <https://doi.org/10.1029/2007JC004200>.
- , V. Mensah, S. Jan, M.-H. Chang, Y.-J. Yang, C. M. Lee, B. Ma, and T. B. Sanford, 2017: Downstream evolution of the Kuroshio's time-varying transport and velocity structure. *J. Geophys. Res. Oceans*, **122**, 3519–3542, <https://doi.org/10.1002/2016JC012519>.
- Chang, M.-H., S. Jan, V. Mensah, M. Andres, L. Rainville, Y.-J. Yang, and Y. H. Cheng, 2018: Zonal migration and transport variations of the Kuroshio east of Taiwan induced by eddy impingements. *Deep-Sea Res. I*, **131**, 1–15, <https://doi.org/10.1016/j.dsr.2017.11.006>.
- Chang, Y.-L., and L.-Y. Oey, 2011: Interannual and seasonal variations of Kuroshio transport east of Taiwan inferred from 29 years of tide-gauge data. *Geophys. Res. Lett.*, **38**, L08603, <https://doi.org/10.1029/2011GL047062>.
- , Y. Miyazawa, and X. Guo, 2015: Effects of the STCC eddies on the Kuroshio based on the 20-year JCOPE2 reanalysis results. *Prog. Oceanogr.*, **135**, 64–76, <https://doi.org/10.1016/j.pocean.2015.04.006>.
- Chao, S.-Y., 1984: Bimodality of the Kuroshio. *J. Phys. Oceanogr.*, **14**, 92–103, [https://doi.org/10.1175/1520-0485\(1984\)014<0092:BOTK>2.0.CO;2](https://doi.org/10.1175/1520-0485(1984)014<0092:BOTK>2.0.CO;2).

- Cheng, Y.-H., C.-R. Ho, Q. Zheng, B. Qiu, J. Hu, and N.-J. Kuo, 2017: Statistical features of eddies approaching the Kuroshio east of Taiwan Island and Luzon Island. *J. Oceanogr.*, **73**, 427–438, <https://doi.org/10.1007/s10872-017-0411-7>.
- Ebuchi, N., and K. Hanawa, 2003: Influence of mesoscale eddies on variations of the Kuroshio paths south of Japan. *J. Oceanogr.*, **59**, 25–36, <https://doi.org/10.1023/A:1022856122033>.
- Gilson, J., and D. Roemmich, 2002: Mean and temporal variability in Kuroshio geostrophic transport south of Taiwan (1993–2001). *J. Oceanogr.*, **58**, 183–195, <https://doi.org/10.1023/A:1015841120927>.
- Hsin, Y.-C., B. Qiu, T.-L. Chiang, and C.-R. Wu, 2013: Seasonal to interannual variations in the intensity and central position of the surface Kuroshio east of Taiwan. *J. Geophys. Res. Oceans*, **118**, 4305–4316, <https://doi.org/10.1002/jgrc.20323>.
- Ichikawa, H., and R. C. Beardsley, 1993: Temporal and spatial variability of volume transport of the Kuroshio in the East China Sea. *Deep-Sea Res. I*, **40**, 583–605, [https://doi.org/10.1016/0967-0637\(93\)90147-U](https://doi.org/10.1016/0967-0637(93)90147-U).
- Ichikawa, K., 2001: Variation of the Kuroshio in the Tokara Strait induced by meso-scale eddies. *J. Oceanogr.*, **57**, 55–68, <https://doi.org/10.1023/A:1011174720390>.
- Imawaki, S., H. Uchida, H. Ichikawa, M. Fukasawa, S. Umatani, and the ASUKA Group, 2001: Satellite altimeter monitoring the Kuroshio transport south of Japan. *Geophys. Res. Lett.*, **28**, 17–20, <https://doi.org/10.1029/2000GL011796>.
- , A. S. Bower, L. Beal, and B. Qiu, 2013: Western boundary currents. *Ocean Circulation and Climate: A 21st Century Perspective*, 2nd ed. G. Siedler et al., Eds., Academic Press, 305–338.
- Ishii, M., Y. Fukuda, H. Hirahara, S. Yasui, T. Suzuki, and K. Sato, 2017: Accuracy of global upper ocean heat content estimation expected from present observational data sets. *SOLA*, **13**, 163–167, <https://doi.org/10.2151/sola.2017-030>.
- Jan, S., V. Mensah, M. Andres, M.-H. Chang, and Y. J. Yang, 2017: Eddy-Kuroshio interactions: Local and remote effects. *J. Geophys. Res. Oceans*, **122**, 9744–9764, <https://doi.org/10.1002/2017JC013476>.
- Joh, Y., and E. Di Lorenzo, 2019: Interactions between Kuroshio Extension and central tropical Pacific lead to preferred decadal timescale oscillations in Pacific climate. *Sci. Rep.*, **9**, 13558, <https://doi.org/10.1038/s41598-019-49927-y>.
- Kawabe, M., 1980: Sea level variations around the Nansei Islands and the large meander in the Kuroshio south of central Japan. *J. Oceanogr. Soc. Japan*, **36**, 227–235, <https://doi.org/10.1007/BF02070336>.
- , 1995: Variations of current path, velocity, and volume transport of the Kuroshio in relation with the large meander. *J. Phys. Oceanogr.*, **25**, 3103–3117, [https://doi.org/10.1175/1520-0485\(1995\)025<3103:VOCPPA>2.0.CO;2](https://doi.org/10.1175/1520-0485(1995)025<3103:VOCPPA>2.0.CO;2).
- Kobashi, F., and H. Kawamura, 2002: Seasonal variation and instability nature of the North Pacific Subtropical Countercurrent and the Hawaiian Lee Countercurrent. *J. Geophys. Res.*, **107**, C03185, <https://doi.org/10.1029/2001JC001225>.
- , and K. Hanawa, 2004: Hydrographic features off the southeast coast of Kyushu during the Kuroshio small meanders: A case study for small meanders that occurred in 1994 and 1995. *J. Oceanogr.*, **60**, 645–661, <https://doi.org/10.1007/s10872-004-5758-x>.
- , H. Mitsudera, and S.-P. Xie, 2006: Three subtropical fronts in the North Pacific: Observational evidence for mode water-induced subsurface frontogenesis. *J. Geophys. Res.*, **111**, C09033, <https://doi.org/10.1029/2006JC003479>.
- Kundu, P. K., I. M. Cohen, and D. R. Dowling, 2016: *Fluid Mechanics*. 6th ed. Academic Press, 921 pp.
- Lien, R.-C., B. Ma, Y.-H. Cheng, C.-R. Ho, B. Qiu, C. M. Lee, and M.-H. Chang, 2014: Modulation of Kuroshio transport by mesoscale eddies at the Luzon Strait entrance. *J. Geophys. Res. Oceans*, **119**, 2129–2142, <https://doi.org/10.1002/2013JC009548>.
- Mantua, N. J., S. R. Hare, Y. Zhang, J. M. Wallace, and R. C. Francis, 1997: A Pacific interdecadal climate oscillation with impacts on salmon production. *Bull. Amer. Meteor. Soc.*, **78**, 1069–1079, [https://doi.org/10.1175/1520-0477\(1997\)078<1069:APICOW>2.0.CO;2](https://doi.org/10.1175/1520-0477(1997)078<1069:APICOW>2.0.CO;2).
- Maximenko, N., 2002: Index and composites of the Kuroshio meander south of Japan. *J. Oceanogr.*, **58**, 639–649, <https://doi.org/10.1023/A:1022886121607>.
- Mitsudera, H., T. Waseda, T. Yoshikawa, and B. Taguchi, 2001: Anticyclonic eddies and Kuroshio meander formation. *Geophys. Res. Lett.*, **28**, 2025–2028, <https://doi.org/10.1029/2000GL012668>.
- Miyazawa, Y., X. Guo, and T. Yamagata, 2004: Roles of mesoscale eddies in the Kuroshio paths. *J. Phys. Oceanogr.*, **34**, 2203–2222, [https://doi.org/10.1175/1520-0485\(2004\)034<2203:ROMEIT>2.0.CO;2](https://doi.org/10.1175/1520-0485(2004)034<2203:ROMEIT>2.0.CO;2).
- , T. Kagimoto, X. Guo, and H. Sakuma, 2008: The Kuroshio large meander formation in 2004 analyzed by an eddy-resolving ocean forecast system. *J. Geophys. Res.*, **113**, C10015, <https://doi.org/10.1029/2007JC004226>.
- Moriyasu, S., 1961: On the difference in the monthly sea level between Kushimoto and Urakami, Japan. *J. Oceanogr. Soc. Japan*, **17**, 197–200, <https://doi.org/10.5928/kaiyou1942.17.197>.
- Na, H., K.-Y. Kim, S. Minobe, and Y. N. Sasaki, 2018: Interannual to decadal variability of the upper-ocean heat content in the western North Pacific and its relationship to oceanic and atmospheric variability. *J. Climate*, **31**, 5107–5125, <https://doi.org/10.1175/JCLI-D-17-0506.1>.
- Noh, Y., B.-Y. Yim, S.-H. You, J.-H. Yoon, and B. Qiu, 2007: Seasonal variation of eddy kinetic energy of the North Pacific Subtropical Countercurrent simulated by an eddy-resolving OGCM. *Geophys. Res. Lett.*, **34**, L07601, <https://doi.org/10.1029/2006GL029130>.
- Qiu, B., 1999: Seasonal eddy field modulation of the North Pacific Subtropical Countercurrent: TOPEX/POSEIDON observations and theory. *J. Phys. Oceanogr.*, **29**, 2471–2486, [https://doi.org/10.1175/1520-0485\(1999\)029<2471:SEFMOT>2.0.CO;2](https://doi.org/10.1175/1520-0485(1999)029<2471:SEFMOT>2.0.CO;2).
- , 2019: Kuroshio and Oyashio currents. *Encyclopedia of Ocean Sciences*, 3rd ed. J. K. Cochran, H. Bokuniewicz, and P. Yager, Eds., Academic Press, 384–394.
- , and W. Miao, 2000: Kuroshio path variations south of Japan: Bimodality as a self-sustained internal oscillation. *J. Phys. Oceanogr.*, **30**, 2124–2137, [https://doi.org/10.1175/1520-0485\(2000\)030<2124:KPVSOJ>2.0.CO;2](https://doi.org/10.1175/1520-0485(2000)030<2124:KPVSOJ>2.0.CO;2).
- , and S. Chen, 2005: Variability of the Kuroshio Extension jet, recirculation gyre and mesoscale eddies on decadal timescales. *J. Phys. Oceanogr.*, **35**, 2090–2103, <https://doi.org/10.1175/JPO2807.1>.
- , and —, 2010a: Eddy-mean flow interaction in the decadal-modulating Kuroshio Extension system. *Deep-Sea Res. II*, **57**, 1098–1110, <https://doi.org/10.1016/j.dsr2.2008.11.036>.
- , and —, 2010b: Interannual variability of the North Pacific Subtropical Countercurrent and its associated mesoscale eddy field. *J. Phys. Oceanogr.*, **40**, 213–225, <https://doi.org/10.1175/2009JPO4285.1>.
- , —, N. Schneider, and B. Taguchi, 2014: A coupled decadal prediction of the dynamic state of the Kuroshio Extension

- system. *J. Climate*, **27**, 1751–1764, <https://doi.org/10.1175/JCLI-D-13-00318.1>.
- , —, —, E. Oka, and S. Sugimoto, 2020: On reset of the wind-forced decadal Kuroshio Extension variability in late 2017. *J. Climate*, **33**, 10 813–10 828, <https://doi.org/10.1175/JCLI-D-20-0237.1>.
- Rio, M.-H., S. Guinehut, and G. Larnico, 2011: New CNES-CLS09 global mean dynamic topography computed from the combination of GRACE data, altimetry, and in situ measurements. *J. Geophys. Res.*, **116**, C07018, <https://doi.org/10.1029/2010JC006505>.
- Risien, C. M., and D. B. Chelton, 2008: A global climatology of surface wind and wind stress fields from eight years of QuickSCAT scatterometer data. *J. Phys. Oceanogr.*, **38**, 2379–2413, <https://doi.org/10.1175/2008JPO3881.1>.
- Solomon, H., 1978: Occurrence of small “trigger” meanders in the Kuroshio off southern Kyushu. *J. Oceanogr. Soc. Japan*, **34**, 81–84, <https://doi.org/10.1007/BF02109256>.
- Sugimoto, S., B. Qiu, and A. Kojima, 2020: Marked coastal warming off Tokai attributable to Kuroshio large meander. *J. Oceanogr.*, **76**, 141–154, <https://doi.org/10.1007/s10872-019-00531-8>.
- Taguchi, B., S.-P. Xie, N. Schneider, M. Nonaka, H. Sasaki, and Y. Sasai, 2007: Decadal variability of the Kuroshio Extension: Observations and an eddy-resolving model hindcast. *J. Climate*, **20**, 2357–2377, <https://doi.org/10.1175/JCLI4142.1>.
- Tsujino, H., N. Usui, and H. Nakano, 2006: Dynamics of Kuroshio path variations in a high-resolution general circulation model. *J. Geophys. Res.*, **111**, C11001, <https://doi.org/10.1029/2005JC003118>.
- , S. Nishikawa, K. Sakamoto, N. Usui, H. Nakano, and G. Yamanaka, 2013: Effects of large-scale wind on the Kuroshio path south of Japan in a 60-year historical OGCM simulation. *Climate Dyn.*, **41**, 2287–2318, <https://doi.org/10.1007/s00382-012-1641-4>.
- Usui, N., H. Tsujino, Y. Fujii, and M. Kamachi, 2008a: Generation of a trigger meander for the 2004 Kuroshio large meander. *J. Geophys. Res.*, **113**, C01012, <https://doi.org/10.1029/2007JC004266>.
- , —, H. Nakano, and Y. Fujii, 2008b: Formation process of the Kuroshio large meander in 2004. *J. Geophys. Res.*, **113**, C08047, <https://doi.org/10.1029/2007JC004675>.
- , —, —, and S. Matsumoto, 2013: Long-term variability of the Kuroshio path south of Japan. *J. Oceanogr.*, **69**, 647–670, <https://doi.org/10.1007/s10872-013-0197-1>.
- Yoon, J.-H., and I. Yasuda, 1987: Dynamics of the Kuroshio large meander: Two-layer model. *J. Phys. Oceanogr.*, **17**, 66–81, [https://doi.org/10.1175/1520-0485\(1987\)017<0066:DOTKLM>2.0.CO;2](https://doi.org/10.1175/1520-0485(1987)017<0066:DOTKLM>2.0.CO;2).
- Yoshida, T., Y. Shimohira, H. Rinno, K. Yokouchi, and H. Akiyama, 2006: Criteria for the determination of a large meander of the Kuroshio based on its path information. *Oceanogr. Japan*, **15**, 499–507.
- Zhang, D., T. N. Lee, W. E. Johns, C.-T. Liu, and R. Zantopp, 2001: The Kuroshio east of Taiwan: Modes of variability and relationship to interior ocean mesoscale eddies. *J. Phys. Oceanogr.*, **31**, 1054–1074, [https://doi.org/10.1175/1520-0485\(2001\)031<1054:TKEOTM>2.0.CO;2](https://doi.org/10.1175/1520-0485(2001)031<1054:TKEOTM>2.0.CO;2).